

**ADVANCING INTEGRATED CO₂ CAPTURE AND
ELECTROCHEMICAL CONVERSION IN DEEP EUTECTIC
SOLVENTS**

CINI M SURESH



**DEPARTMENT OF CHEMISTRY
INDIAN INSTITUTE OF TECHNOLOGY DELHI
JULY 2025**

© Indian Institute of Technology Delhi (IITD), New Delhi, 2025

Advancing Integrated CO₂ Capture and Electrochemical Conversion in Deep Eutectic Solvents

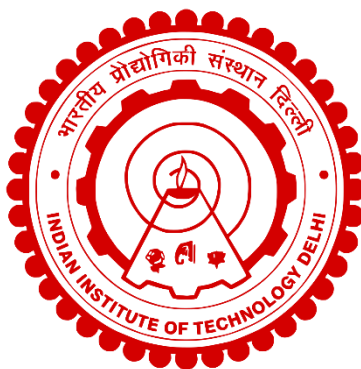
by

**Cini M Suresh
Department of Chemistry**

Submitted

**in fulfilment of the requirements of the degree of
Doctor of Philosophy**

to the



**Indian Institute of Technology Delhi
July 2025**

Dedicated to

Elias — for making the journey easier

My family — for being the shoulders I stand upon

CERTIFICATE

This is to certify that the thesis entitled “**Advancing Integrated CO₂ Capture and Electrochemical Conversion in Deep Eutectic Solvents**” being submitted by Ms. Cini M. Suresh to the Indian Institute of Technology, Delhi, for the award of the degree of Doctor of Philosophy in Chemistry, is a record of bonafide research work carried out by her. She has worked under my supervision and has fulfilled the requirements, which, to my knowledge, has reached the requisite standard for submitting the thesis. The results in this thesis have not been submitted to any other university or institute, whether in part or full, for the awards of any other degree or diploma.

Prof. Pravin P. Ingole Professor,
Department of Chemistry
Indian Institute of Technology
Hauz Khas,
New Delhi – 110016

ACKNOWLEDGEMENTS

With a heart full of gratitude, I begin by acknowledging the grace and mercies of God Almighty. The verse from Colossians 3:17, *“And whatever you do, in word or deed, do everything in the name of the Lord Jesus, giving thanks to God the Father through him,”* has continually reminded me of the purpose behind my work, encouraging me to live this life to the fullest with faith and gratitude.

Though the pursuit of a PhD is intensely personal, it is shaped profoundly by the people who surround and support us along the way. To everyone who contributed to my journey, whether named here or not, you hold a cherished place in my heart.

I express my deepest appreciation to my supervisor, who entrusted me with the opportunity to embark on this academic journey. His mentorship provided the space and support needed for original research, has been invaluable. I remain inspired by his dedication to both scientific excellence and community service. I would also like to thank my SRC members, Prof. Sameer Sapra, Prof. Hemant Kashyap, and Prof. Anil Verma for their invaluable insights, which refined my work to meet the standards of this esteemed institution. A special note of thanks to Prof. Hemant Kashyap and his student Mirtyunjay, with whom I had the pleasure of collaborating on theoretical aspects of two projects. The Heads of the Department during my tenure: Prof. Anil J. Elias, Prof. Narayanan Kurur, Prof. Sidharth Pandey, and Prof. S. Nagendran, deserve acknowledgment for steering the department with diligence and vision. I also thank the Chemistry departmental office staff, DRC members whose efficiency and kindness smoothed countless administrative processes over the years. I am grateful for the excellent instrumentation facilities and operators at IIT Delhi, including those managed by the Chemistry Department, CRF, and NRF. My appreciation also extends to the IIT Delhi administration for organizing numerous academic and co-curricular events that enriched my overall experience. I was fortunate to collaborate with Ms Bipasa Dey and Prof. Tanmay Dutta. Our interdisciplinary discussions at the intersection of biochemistry and electrochemistry led to meaningful research contributions.

Being part of a vibrant lab community has been a blessing. My heartfelt thanks to my seniors, Dr. Nusrat Rashid, Dr. Preeti Choudhary, Dr. Shwetambara Jha, Dr. Rasmita Barik, Dr. Vaishali Tanwar, Dr. Priya Jain, and Dr. Jyoti Rohilla, whose strength, clarity, and pioneering efforts laid the groundwork for much of our current research. To my colleagues and friends Ajai, Aejaz, Aamir,

and Navneet, thank you for the camaraderie, encouragement, and countless conversations that brought perspective and comfort during trying times. They have been a constant source of emotional support through the roller coaster of paper rejections and acceptances. Aejaz's deep passion for electrochemistry and willingness to engage in scientific dialogue inspired and guided my own understanding. Navneet, working closely in a similar domain, provided intellectual companionship and was a co-author on two key projects, his presence made the new research direction on reactive CO₂ capture more navigable. Thanks to Shivangi, Jagriti, Bhawana, Darshana, and Roshan for leading fun lab events and infusing energy into our work environment.

Outside the academic sphere, Delhi gifted me with friendships that I will treasure for a lifetime. Shreya, my first friend and roommate at IITD, was always a call away, for spontaneous chai breaks, heartfelt talks, and shared laughter. The EU fellowship community and the student prayer group were a vital support system, our collective faith, shared meals, Bible studies, and celebrations added joy to even the most difficult days. I am also grateful to my church family in Delhi, whose fellowship, prayers, and warm hospitality were a steady source of strength. Special thanks to Rachel, Kiruba, and little Kiara for making life in Delhi feel like home.

My deepest gratitude goes to my family. My father, steadfast in prayer, would kneel in intercession during every exam and presentation. His example of perseverance and commitment continues to inspire me. My mother, with her constant love and care, made even the most challenging days bearable. My sister, my lifelong best friend, has shared in my joys and sorrows with unmatched empathy. I am also thankful to my in-laws for their encouragement, love, and belief in me. The extended support from my cousins, aunts, uncles, and grandparents rejuvenated my spirit during visits home, and the little kids of the family were a continuous source of joy.

Finally, my deepest love and thanks to my husband, Elias. Being married to a PhD student is not for the weak-hearted. I was uncertain how pursuing a PhD post-marriage would unfold, but Elias's unwavering support, delicious meals, boundless affection, and steadfast presence have been my anchor. His companionship brought warmth and joy to each day, and I eagerly look forward to journeying through life's adventures with him by my side.

Cini

ABSTRACT

The unprecedented increase in atmospheric CO₂ levels, primarily driven by anthropogenic emissions, poses a major global challenge. Simultaneously, carbon dioxide represents an abundant and underutilized C-feedstock that can be converted into valuable fuels and platform chemicals. This duality has given rise to intense research interest in carbon capture and utilization (CCU) technologies. However, most current CCU strategies treat capture and conversion as discrete processes, with traditional thermal CO₂ regeneration methods proving energetically demanding and inefficient. In this context, electrochemical reactive CO₂ capture (eRCC) presents a promising integrated alternative, one that merges the capture and conversion steps, thus lowering energy input and enabling on-demand valorization of captured CO₂ under mild conditions. A core challenge in implementing eRCC lies in identifying or engineering an electrolyte system that not only ensures high CO₂ solubility and favorable reaction kinetics but also supports a wide electrochemical window and stable operation. Deep eutectic solvents (DESs), a novel class of designer solvents formed from mixtures of hydrogen bond donors (HBDs) and acceptors (HBAs), offer remarkable tunability in their physicochemical properties, making them attractive candidates for eRCC media. This thesis investigates the utility of DESs for electrochemical CO₂ capture and conversion, with particular focus on their interfacial behavior, bulk properties, and synergistic role in paired electrocatalytic systems.

Chapter 1 introduces the conceptual and scientific background motivating this work. It discusses the urgency of developing sustainable CO₂ management technologies and the emerging role of reactive CO₂ capture strategies. A comprehensive review of various reactive capture approaches is presented, highlighting both the promise and the limitations of current systems. The unique advantages of electrochemical reactive CO₂ capture are justified, particularly its potential to minimize energetic penalties and enable decentralized applications. The rationale for selecting DESs as the electrolyte framework is also presented, followed by a clear statement of the research objectives and an overview of the thesis structure.

Chapter 2 provides a detailed description of the experimental methodologies and characterization techniques employed throughout the study. Key electrochemical techniques—cyclic voltammetry (CV), electrochemical impedance spectroscopy (EIS), and chronoamperometry (CA)—were used to probe electrochemical behavior and monitor catalytic performance.

To quantify CO₂ reduction products, gas chromatography (GC) was used for gaseous species, while nuclear magnetic resonance (NMR) spectroscopy was employed for liquid-phase products. The structural and morphological evolution of metal foil electrodes during electrolysis was studied using scanning electron microscopy (SEM), field-emission SEM (FESEM), X-ray diffraction (XRD), Fourier-transform infrared spectroscopy (FTIR), Raman spectroscopy, and X-ray photoelectron spectroscopy (XPS). Gravimetric CO₂ capture measurements leveraged the non-volatile nature of DESs, and ¹³C NMR alongside FTIR spectroscopy were used to explore the chemical mechanisms underlying CO₂ absorption. The chapter also outlines the procedures for DES preparation, catalyst synthesis, and the instrumental setups used across the thesis.

Chapter 3 explores the influence of DES composition on eRCC performance by examining the molecular interactions and structure at the electrode–electrolyte interface. A tailored DES system (Ethaline), modified with the addition of the organic superbases DBU to enhance CO₂ affinity and dimethyl sulfoxide (DMSO) to reduce viscosity, was developed and evaluated. Through both experimental and computational analysis, the study reveals that CO₂ capture and conversion performance in such DESs is governed by a complex interplay of factors: the availability of reactive sites, mass transport influenced by viscosity and conductivity, CO₂–DES interaction energies, and the structure of the electrochemical double layer (EDL). The results suggest that the local microenvironment at the Cu/DES interface is highly sensitive to DES formulation and critically determines the efficiency and selectivity of CO₂ conversion reactions.

Chapter 4 focuses on systematically tuning the hydrogen bond donor component of type III DESs to understand its effect on bulk and interfacial properties relevant to eRCC. A range of HBDs with varying functional groups and molecular structures, including 1,4-butanediol, cresol, levulinic acid, and phenol were paired with choline chloride to create a series of DESs. These modifications significantly influenced DES parameters such as viscosity, CO₂ solubility, and free volume. Changes in HBD structure also altered the EDL structure and the distance of closest approach of reactive species to the electrode surface, ultimately impacting the stabilization of key intermediates during electrocatalysis. Using Au as the working electrode, the study identified how subtle variations in HBD functionality can modulate product formation pathways and efficiency.

Chapter 5 transitions to the role of the electrocatalyst in enhancing eRCC performance. Copper, known for its ability to catalyze CO₂ reduction to hydrocarbons and multi-carbon products, was

chosen as the model electrocatalyst. Nanostructured Cu electrodes were synthesized via pulse galvanostatic electrodeposition from baths containing different copper salts, acetate, chloride, nitrate, and sulfate allowing control over particle morphology and surface characteristics. The study demonstrates that chloride-based precursors lead to the formation of catalytically active Cu₂O/Cu phases with well-defined cubic morphology and enhanced surface area, facilitating higher CO₂ adsorption and activation. Among the variants studied, copper deposited from chloride precursors exhibited the best performance, attributed to favorable surface structure and the presence of subsurface oxygen species. These catalysts were then tested in DES media to assess their morphological stability and electrocatalytic activity under eRCC conditions, offering insights into the design of stable nanocatalysts for DES-based applications.

Chapter 6 investigates the integration of biomass valorization with CO₂ reduction to further enhance process sustainability. Traditionally, water oxidation to O₂ is used as the anodic reaction during CO₂ reduction; however, its high overpotential and limited product value reduces the overall system efficiency. As an alternative, lignin oxidation - a reaction with lower thermodynamic requirements was coupled with CO₂ reduction in a paired electrolysis setup. Lignin oxidation was carried out on a Ni foam electrode, while formic acid production from CO₂ was targeted at the Sn electrode. The paired configuration achieved substantial reductions in cell voltage compared to the conventional HER-OER pairing, and the formation of value-added products. This represents the first demonstration of such a system, highlighting the potential for DES-based electrochemical platforms to drive synergistic carbon and biomass valorization under mild conditions.

Chapter 7 concludes the thesis by summarizing the major findings and discussing their broader implications for the development of integrated CO₂ capture and conversion systems. The study establishes deep eutectic solvents as highly versatile and effective media for electrochemical CO₂ conversion, offering opportunities for rational solvent design, interfacial engineering, and reaction coupling. Future directions are proposed, including the scaling of DES systems to flow cells systems, the integration of renewable energy sources, and the thorough exploration of in-situ electrocatalyst restructuring to maximize energy and carbon efficiency.

ABSTRACT (Hindi)

वायुमंडलीय CO₂ स्तर में अभूतपूर्व वृद्धि, जो मुख्यतः मानवजनित उत्सर्जनों के कारण हो रही है, एक गंभीर वैश्विक चुनौती बन गई है। साथ ही, कार्बन डाइऑक्साइड एक प्रचुर मात्रा में उपलब्ध और अभी तक अपर्याप्त रूप से उपयोग की गई C-फ़ीडस्टॉक है, जिसे मूल्यवान ईंधनों और रासायनिक यौगिकों में रूपांतरित किया जा सकता है। इस दृष्टिकोण ने कार्बन कैप्चर और उपयोग (CCU) तकनीकों में तीव्र अनुसंधान रुचि को जन्म दिया है। हालांकि, वर्तमान CCU रणनीतियाँ आमतौर पर कैप्चर और रूपांतरण को दो पृथक प्रक्रियाओं के रूप में देखती हैं, और पारंपरिक तापीय CO₂ विमोचन विधियाँ ऊर्जा की दृष्टि से अत्यधिक मांग वाली और अलाभकारी सिद्ध होती हैं।

इस परिप्रेक्ष्य में, इलेक्ट्रोरासायनिक प्रतिक्रियाशील CO₂ कैप्चर (eRCC) एक आशाजनक एकीकृत विकल्प के रूप में उभरता है, जो कैप्चर और रूपांतरण दोनों चरणों को एक ही इलेक्ट्रोरासायनिक प्लेटफ़ॉर्म में समाहित करता है। यह ऊर्जा आवश्यकताओं को कम करता है और कोमल परिस्थितियों में CO₂ के मूल्यवर्धन को सक्षम बनाता है। eRCC को लागू करने में एक मुख्य चुनौती ऐसा इलेक्ट्रोलाइट सिस्टम खोजना या विकसित करना है जो उच्च CO₂ विलेयता, अनुकूल प्रतिक्रिया गति, विस्तृत इलेक्ट्रोरासायनिक विंडो और स्थिर संचालन सुनिश्चित कर सके। डीप यूटेक्टिक सॉल्वेंट्स (DESs), जो हाइड्रोजन बॉन्ड डोनर (HBDs) और एक्सेप्टर (HBA_s) के मिश्रण से बनते हैं, ऐसे डिज़ाइनर सॉल्वेंट्स का एक नया वर्ग हैं जिनके भौतिक-रासायनिक गुणों को अत्यधिक समायोजित किया जा सकता है। ये eRCC माध्यम के रूप में अत्यंत आकर्षक विकल्प प्रदान करते हैं।

यह शोध प्रबंध DESs के उपयोग की जांच करता है, विशेष रूप से उनके इंटरफ़ेस व्यवहार, बल्क गुणों और युग्मित इलेक्ट्रोकेटालिटिक प्रणालियों में सहक्रियात्मक भूमिका पर ध्यान केंद्रित करते हुए।

अध्याय 1 इस कार्य की वैचारिक और वैज्ञानिक पृष्ठभूमि प्रस्तुत करता है। इसमें सतत CO₂ प्रबंधन तकनीकों के विकास की आवश्यकता और प्रतिक्रियाशील CO₂ कैप्चर रणनीतियों की उभरती भूमिका पर चर्चा की गई है। विभिन्न प्रतिक्रियाशील कैप्चर दृष्टिकोणों की व्यापक समीक्षा की गई है, जो वर्तमान प्रणालियों की संभावनाओं और सीमाओं दोनों को उजागर करती है। इलेक्ट्रोरासायनिक प्रतिक्रियाशील CO₂ कैप्चर की विशिष्ट विशेषताओं को उचित ठहराया गया है, विशेष रूप से इसके ऊर्जा हानि को न्यूनतम करने और विकेंद्रित अनुप्रयोगों में सक्षम होने की क्षमता के संदर्भ में। DESs को इलेक्ट्रोलाइट ढांचे के रूप में चुनने का तर्क और शोध के उद्देश्य तथा प्रबंध की संरचना का अवलोकन भी प्रस्तुत किया गया है।

अध्याय 2 अध्ययन में प्रयुक्त प्रयोगात्मक कार्यप्रणालियों और विशेषता तकनीकों का विस्तृत विवरण प्रदान करता है। प्रमुख इलेक्ट्रोरासायनिक तकनीकें—साइक्लिक वोल्टमेट्री (CV), इलेक्ट्रोरासायनिक प्रतिबाधा स्पेक्ट्रोस्कोपी (EIS), और क्रोनोएम्पेरोमेट्री (CA)—का उपयोग इलेक्ट्रोरासायनिक व्यवहार की जांच और उत्प्रेरक प्रदर्शन की निगरानी के लिए किया गया। CO₂ अपचयन उत्पादों की मात्रा निर्धारण के लिए गैसीय उत्पादों हेतु गैस क्रोमैटोग्राफी (GC) और द्रव उत्पादों हेतु न्यूक्लियर मैग्नेटिक रेजोनेंस (NMR) स्पेक्ट्रोस्कोपी का उपयोग किया गया। इलेक्ट्रोलिसिस के दौरान धातु फॉयल इलेक्ट्रोड्स के संरचनात्मक और रूपात्मक विकास का अध्ययन SEM, FESEM, XRD, FTIR, Raman स्पेक्ट्रोस्कोपी और XPS के माध्यम से किया गया। CO₂ कैप्चर मापनों के लिए DESs की अवाष्पशील प्रकृति का लाभ उठाया गया, और ¹³C NMR तथा FTIR का उपयोग CO₂ अवशोषण की रासायनिक प्रक्रियाओं की जांच के लिए किया गया। इस अध्याय में DES निर्माण, उत्प्रेरक संश्लेषण और उपकरणिय सेटअप की प्रक्रियाएँ भी वर्णित हैं।

अध्याय 3 DES संरचना के eRCC प्रदर्शन पर प्रभाव की जांच करता है, विशेष रूप से इलेक्ट्रोड-इलेक्ट्रोलाइट इंटरफेस पर अंतरफलक संरचना और आणविक पारस्परिक क्रियाओं के संदर्भ में। एक विशेष रूप से तैयार किया गया DES सिस्टम (Ethaline), जिसमें CO₂ के प्रति आकर्षण बढ़ाने हेतु ऑर्गेनिक सुपरबेस DBU और चिपचिपाहट कम करने के लिए डाईमिथाइल सल्फ़ोक्साइड (DMSO) मिलाया गया, का विकास और मूल्यांकन किया गया। प्रयोगात्मक और संगणकीय विश्लेषण से यह पता चला कि इन DESs में CO₂ कैप्चर और रूपांतरण का प्रदर्शन विभिन्न जटिल कारकों के संयोजन द्वारा निर्धारित होता है: प्रतिक्रियाशील साइटों की उपलब्धता, चिपचिपाहट और चालकता द्वारा प्रभावित द्रव्य परिवहन, CO₂-DES इंटरैक्शन ऊर्जा, और इलेक्ट्रोरासायनिक डबल लेयर की संरचना। परिणाम बताते हैं कि Cu/DES इंटरफ़ेस पर स्थानीय सूक्ष्म वातावरण DES संरचना के प्रति अत्यधिक संवेदनशील होता है और CO₂ रूपांतरण प्रतिक्रिया की दक्षता और चयनात्मकता को नियंत्रित करता है।

अध्याय 4 प्रकार III DESs में हाइड्रोजन बॉन्ड डोनर घटक को व्यवस्थित रूप से समायोजित करता है ताकि eRCC से संबंधित बल्क और इंटरफेस गुणों पर उसके प्रभाव को समझा जा सके। विभिन्न कार्यात्मक समूहों और आणविक संरचनाओं वाले HBDs जैसे 1,4-ब्यूटेनडायोल, क्रेसोल, लेवुलिनिक एसिड और फिनोल को कोलाइन क्लोराइड के साथ मिलाकर DESs की एक श्रृंखला तैयार की गई। इन संशोधनों ने चिपचिपाहट, CO₂ विलेयता और मुक्त आयतन जैसे गुणों को प्रभावित किया। HBD संरचना में बदलावों ने EDL संरचना और प्रतिक्रियाशील प्रजातियों की इलेक्ट्रोड सतह तक पहुंच की दूरी को भी परिवर्तित किया, जिससे

इलेक्ट्रोकेटलिसिस के दौरान प्रमुख मध्यवर्ती उत्पादों की स्थिरीकरण प्रक्रिया पर प्रभाव पड़ा। Au इलेक्ट्रोड के उपयोग से यह समझा गया कि HBD कार्यात्मकता में सूक्ष्म परिवर्तन भी उत्पाद बनने के मार्ग और दक्षता को प्रभावित कर सकते हैं।

अध्याय 5 eRCC प्रदर्शन को बेहतर बनाने में इलेक्ट्रोकेटलिस्ट की भूमिका पर केंद्रित है। तांबा (Cu), जो CO₂ को हाइड्रोकार्बन और बहु-कार्बन उत्पादों में रूपांतरित करने की क्षमता रखता है, को मॉडल उत्प्रेरक के रूप में चुना गया। विभिन्न तांबे लवणों—एसीटेट, क्लोराइड, नाइट्रेट और सल्फेट—से युक्त सानों से पल्स गैल्वेनोस्टैटिक इलेक्ट्रोडिपोजिशन द्वारा नैनोसंरचित Cu इलेक्ट्रोड्स का संश्लेषण किया गया, जिससे कण आकारिकी और सतह विशेषताओं को नियंत्रित किया जा सके। अध्ययन दर्शाता है कि क्लोराइड आधारित प्रीकर्सर्स से Cu₂O/Cu चरणों का गठन होता है जिनकी घनाकार संरचना और उच्च सतह क्षेत्र होता है, जिससे CO₂ का बेहतर अवशोषण और सक्रियण संभव होता है। इन इलेक्ट्रोड्स को DES माध्यम में परीक्षण किया गया जिससे इनकी संरचनात्मक स्थिरता और इलेक्ट्रोकेटलिटिक गतिविधि पर अंतर्दृष्टि प्राप्त हुई।

अध्याय 6 CO₂ अपचयन को अधिक सतत बनाने के लिए बायोमास वैलराइजेशन के एकीकरण की जांच करता है। पारंपरिक रूप से CO₂ अपचयन के दौरान एनोड पर जल का ऑक्सीकरण होता है जिससे O₂ बनता है, लेकिन यह उच्च ओवरपोटेंशियल और कम उत्पाद मूल्य के कारण प्रणाली की दक्षता को कम करता है। एक विकल्प के रूप में, कम ऊष्मागतिकीय आवश्यकता वाले लिग्निन ऑक्सीकरण को CO₂ अपचयन के साथ युग्मित किया गया। Ni फोम इलेक्ट्रोड पर लिग्निन ऑक्सीकरण और Sn इलेक्ट्रोड पर फॉर्मिक एसिड निर्माण को लक्षित किया गया। इस युग्मित विन्यास ने पारंपरिक HER-OER संयोजन की तुलना में सेल वोल्टेज को काफी हद तक कम किया और मूल्यवर्धित उत्पादों का निर्माण किया। यह प्रणाली DES आधारित इलेक्ट्रोरासायनिक प्लेटफार्मों की क्षमता को दर्शाती है जो कोमल परिस्थितियों में कार्बन और बायोमास वैलराइजेशन को सक्षम बनाती है।

अध्याय 7 इस शोध प्रबंध का समापन करते हुए प्रमुख निष्कर्षों को संक्षेपित करता है और एकीकृत CO₂ कैचर और रूपांतरण प्रणालियों के विकास पर उनके व्यापक प्रभावों की चर्चा करता है। यह अध्ययन दर्शाता है कि DESs इलेक्ट्रोरासायनिक CO₂ रूपांतरण के लिए अत्यधिक बहुपरक और प्रभावी माध्यम हो सकते हैं, जिससे सॉल्वेंट डिज़ाइन, इंटरफेस इंजीनियरिंग और प्रतिक्रिया युग्मन के नए अवसर उत्पन्न होते हैं। भविष्य की दिशा में DES प्रणालियों का स्केल-अप, नवीकरणीय ऊर्जा स्रोतों का एकीकरण, और ऊर्जा व कार्बन दक्षता को अधिकतम करने के लिए अतिरिक्त युग्मित प्रतिक्रियाओं की खोज प्रस्तावित की गई है

TABLE OF CONTENTS

CERTIFICATE	iii
ACKNOWLEDGEMENT	iv
ABSTRACT	vi
TABLE OF CONTENTS	xii
LIST OF FIGURES	xvi
LIST OF TABLES	xxv
ABBREVIATIONS AND SYMBOLS	xxvi
CHAPTER 1. Introduction	
1.1 CO ₂ Capture and Utilisation	2
1.1.1 CO ₂ capture media	3
1.1.2 CO ₂ conversion methods	5
1.2 Electrochemical CO ₂ reduction and its challenges	8
1.3 Reactive CO ₂ capture	10
1.3.1 Electrochemical reactive CO ₂ capture	12
1.4 Deep Eutectic Solvents	14
1.5 Advancing electrochemical reactive CO ₂ capture in DES: Opportunities and Gap area	17
1.5.1 Optimizing bulk interactions to increase CO ₂ capture	17
1.5.2 Optimizing electrochemical interfacial structure to enhance CO ₂ conversion	20
1.5.3 CO ₂ activation and HER suppression	23
1.5.4 Electrode/Electrocatalyst stability in and restructuring DES	24
1.5.5 Counter reactions to eRCC in DES	25
1.6 Scope and Objectives	26
1.7 Thesis Structure and Organization	26
1.8 References	28
CHAPTER 2: Materials and Experimental Methodology	
2.1 Electrolyte Engineering	40
2.1.1 Preparation of Deep Eutectic Solvents	40
2.1.2 Solvent pre-electrolysis treatment and storage	42
2.1.3 Solvent characterization techniques	44
2.1.4 Physico-chemical properties measurements	46
2.2 CO ₂ capture measurements	50
2.2.1 Gravimetric analysis	50
2.2.2 Understanding CO ₂ capture state and interactions with DES	51
2.3 Electrocatalyst modification	54

2.3.1	Metal foil (electrode) pre-treatment	54
2.3.2	Synthesis of Cu electrodeposits	54
2.3.3	Structural characterization	56
2.3.4	Morphological characterization	56
2.4	Electrochemical set-up	60
2.4.1	Electrode fabrication	61
2.4.2	Electrolytes	61
2.4.3	Electrochemical cell	62
2.4.4	Membrane cleaning and activation	64
2.4.5	Data recording and handling	64
2.4.6	Electrode-electrocatalyst stability test	66
2.5	Electrochemical techniques	67
2.5.1	Cyclic and linear sweep voltammetry	67
2.5.2	Electrochemical Impedance Spectroscopy	69
2.5.3	Chronoamperometry and chronopotentiometry	71
2.5.4	Differential Capacitance measurements	71
2.6	Electrolysis product quantification methods	72
2.6.1	CO ₂ electrolysis gaseous product quantification	72
2.6.2	CO ₂ electrolysis liquid product quantification	74
2.6.3	Electrochemical oxidative lignin depolymerization product quantification	76
2.7	Conclusion	84
2.8	References	85
CHAPTER 3: DES modification by ternary addition		89
3.1	Abstract	90
3.2	Introduction	91
3.3	Results and discussions	92
3.3.1	Characterization and CO ₂ capture in as-prepared DES	92
3.3.2	Understanding molecular interactions in DES-CO ₂ via AIMD	97
3.3.3	Electrochemical CO ₂ reduction in DES-based electrolytes	103
3.3.4	Control experiments	109
3.3.5	Electrode-electrolyte stability test	112
3.3.6	Discussions	114
3.4	Conclusions	120
3.5	References	121
CHAPTER 4: DES modification by changing HBD		125
4.1	Abstract	126
4.2	Introduction	127

4.3	Results and discussions	128
4.3.1	Characterization and CO ₂ capture in as-prepared DES	128
4.3.2	Electrochemical CO ₂ reduction in DES-based electrolyte	134
4.3.3	Control experiments	138
4.3.4	Discussions	141
4.4	Conclusion	146
4.5	References	147
CHAPTER 5: Electrocatalyst modification		151
5.1	Abstract	152
5.2	Introduction	153
5.3	Results and discussions	154
5.3.1	Structural and morphological characterisation	154
5.3.2	Electrochemical CO ₂ reduction on the electrodeposits	160
5.3.3	Stability of the Cu electrodeposits	164
5.3.4	Discussions	167
5.3.5	Cu-electrodeposits restructuring in DES	170
5.4	Conclusion	171
5.5	References	172
CHAPTER 6: Enhancing overall cell efficiency		179
6.1	Abstract	180
6.2	Introduction	181
6.3	Results and discussions	183
6.3.1	Characterization of lignin	183
6.3.2	Electrochemical set-up description	184
6.3.3	Electrochemical CO ₂ reduction in aqueous electrolyte	185
6.3.4	Electrochemical lignin oxidative depolymerization in aqueous solvents	186
6.3.5	Evaluating the performance of full cell in aqueous electrolyte	187
6.3.6	Electrochemical CO ₂ reduction in DES	188
6.3.7	Electrochemical lignin oxidative depolymerization in DES-based electrolyte	189
6.3.8	Evaluating the performance of the integrated system in DES-based electrolyte	191
6.3.9	Stability of the system	194
6.3.10	Discussions	195
6.4	Conclusion	199
6.5	References	200

CHAPTER 7: Summary and future perspectives	205
7.1 Summary	206
7.1.1 Optimizing the capture and conversion efficiency by changing the constituents of the Deep Eutectic Solvents.	206
7.1.2 Increasing the conversion efficiency and selectivity of electrochemical CO ₂ reduction by optimising the characteristics of Cu-nanostructured electrocatalysts	206
7.1.3 Advancing the electrochemical reactive CO ₂ capture by integrating an efficient oxidation counterpart reaction (Lignin oxidative depolymerization reaction) to increase the efficiency of the full cell	207
7.2 Future scope and perspectives	208
APPENDICES	211
Appendix A	211
Appendix B	215
Appendix C	218
Appendix D	222
CURRICULUM VITAE	226

LIST OF FIGURES

Figure No.	Figure caption	Page No.
1.1	The graph showing monthly mean carbon dioxide globally averaged over marine surface sites.	2
1.2	A schematic representation of CO ₂ capture, either from point sources or direct air capture of the CO ₂ which is uncaptured. The step includes the transportation of the captured CO ₂ which is either stored or utilized for the formation of other value-added chemicals.	3
1.3	The various CO ₂ capture methods via liquid solvents, solid sorbents or membrane separation technology.	4
1.4	The various methods for conversion of CO ₂ into value added products.	7
1.5	(a) A representation of free energy landscape showing the variations in energy utilization during conversion of CO ₂ regenerated from the capture media and the direct conversion of captured CO ₂ (CO ₂ adduct). (b) Number of publications on reactive CO ₂ capture – data exported from Scifinder.	11
1.6	Schematic representation of the difference between sequential CO ₂ capture and conversion and integrated CO ₂ capture and conversion.	12
1.7	(a) Tuning the electrochemical double layer to facilitate reduction of CO ₂ -amine adduct. (b) Increase in conversion efficiency in terms of faradaic efficiency and reaction rate when the electrolyser temperature is increased from 15°C to 75°C.	13
1.8	(a) Eutectic formation when HBA and HBD are mixed in eutectic molar ratio to form a mixture existing in liquid state at room temperature. (b) Schematic representation of the application of DESs.	15
1.9	A schematic representation of CO ₂ captured in DES and the various factors that influence the capture capacity and	18
1.10	Schematic representation of the various that effect the tuning of electrified DES interfaces.	21
1.11	A schematic showing how free energy of the system is decreased in IL EMIM-BF ₄ with respect to in aqueous or acetonitrile systems. Copyright ref ¹⁰⁹ (b) proposed model of the double layer at the electrode interface influenced by various aqueous Reline components. Copyright Ref ⁷²	24
1.12	A schematic representation of the areas of focus and thesis structure.	25
2.1	Schematic representation of the NMR components and its working principle.	45

2.2	(a) Picture of the FTIR instrument used in this thesis. (b) Schematic representation of the working principle of FTIR	45
2.3	(a) Picture of the viscometer used for the experiments in the thesis and (b) a graphical representation of the movement of the ball through the capillary and the forces involved.	48
2.4	Karl Fischer titration instrument used for water detection in the thesis	49
2.5	Schematic representation of the set-up for CO ₂ capture capacity measurement	49
2.6	The experimental set-up for in-situ FTIR (ATR) measurements.	52
2.7	Representative snapshots of equilibrated (left panel) Eth+DBU+CO ₂ and (right panel) Eth+DBU+DMSO+CO ₂ systems. Here, bonds of CH ⁺ , EG, DBU, and DMSO molecules are depicted in ice blue, mauve, orange, and lime colors, respectively. Here, hydrogen, carbon, nitrogen, oxygen, sulfur atoms and chloride ions are depicted in white, cyan, blue, red, yellow, and green colors, respectively.	53
2.8	Schematic representation of the growth of the Cu electrodeposits.	55
2.9	(a) Picture of the Bruker D8 advance XRD instrument used in the thesis and (b) a simple schematic representation of the working principle of XRD.	56
2.10	A picture of the HORIBA, Olympus BX 41 Raman Spectrometer used for analysis used in this thesis.	58
2.11	Schematic representation of the setup for electrochemical CO ₂ reduction.	61
2.12	Schematic representation of 3-electrode and 2 electrode connections	63
2.13	Characteristic (a) CV and (b) LSV curves featuring reduction and oxidation peaks.	68
2.14	(a) The Nyquist plot of a Randle's circuit and (b) the corresponding circuit elements.	70
2.15	(a) Gas chromatogram (GC) FID signals of standard gas mixture (CO- 5130 ppm; CH ₄ – 5115 ppm; CO ₂ - 5138 ppm; C ₂ H ₆ - 5142 ppm; and C ₂ H ₄ - 5148 ppm) (b) enlarged view of the GC-FID signal for the CO ₂ reduction products for a typical reaction on Cu electrode	73
2.16	Representative NMR graphs of formic acid detection in (a) aqueous electrolyte with water suppression and DMSO as internal standard (b) Ethaline-DES as electrolyte and 1,2,4,5-tetrachlorobenzene as internal standard.	74

2.17	Calibration curves of (a) formic acid in 0.2M KHCO ₃ with respect to DMSO as internal standard, (b) formic acid in tailored Ethaline DES-based electrolyte with respect to phenol as internal standard and (c) formic acid in Ethaline with respect to 1,2,4,5- tetrachlorobenzene as internal standard.	76
2.18	(a) Photo of Liquid-liquid extraction (LLE) in separating funnel (b) photo of KOH-lignin solution pre and post electrolysis (c) photo Eth-lignin pre and post electrolysis.	77
2.19	Representative GC-MS graphs of (c) Lignin monomers detected after electrolysis in KOH electrolyte (d) Lignin monomers detected after electrolysis in ethaline electrolyte	78
2.20	Calibration curves of each of the lignin monomer identified	84
Scheme 3.1	Ball-and-stick illustration of the species present in the studied systems: (a) ChCl, (b) EG, (c) CO ₂ , (d) DBU, and (e) DMSO. Here, hydrogen, carbon, nitrogen, oxygen, sulfur atoms and chloride ions are depicted in white, cyan, blue, red, yellow, and green colors, respectively	93
3.1	¹ H NMR of the (a) ethylene glycol, (b) choline chloride, and (c) DBU.	94
3.2	(a) CO ₂ capture capacity, and (b) viscosity and conductivity (under Ar and CO ₂ saturated conditions) of the DES and tailored DES solvent systems.	95
3.3	(a) ¹³ C NMR of the solvents before (black curve) and after CO ₂ (red curve) capture. (b) in-situ IR graphs taken during CO ₂ purging in the solvent systems.	97
3.4	RDFs for (a) C _{CO₂} -OH _{EG} , (b) O _{CO₂} -OH _{EG} (c) C _{CO₂} -Cl ⁻ , (d) O _{CO₂} -Cl ⁻ , (e) C _{CO₂} -N _{[Ch]⁺} , (f) O _{CO₂} -N _{[Ch]⁺} , (g) O _{CO₂} -HO _{[Ch]⁺} , and (h) O _{CO₂} -OH _{[Ch]⁺} atomic pairs in Eth+DBU and Eth+DBU+DMSO having CO ₂ . The RDFs are compared with previously published data for Eth+CO ₂ system by Malik <i>et al</i> ²⁶ . Here, C _{CO₂} and O _{CO₂} are carbon and oxygen atoms of CO ₂ , respectively. OH _{EG} is the hydroxyl oxygen atom of EG. N _{[Ch]⁺} and OH _{[Ch]⁺} represent nitrogen and hydroxyl oxygen of Ch ⁺ , respectively.	99
3.5	Solvation RDFs for (a) C _{CO₂} -N _{1DBU} , C _{CO₂} -N _{2DBU} , (b) O _{CO₂} -N _{1DBU} , O _{CO₂} -N _{2DBU} in Eth+DBU+CO ₂ , (c) C _{CO₂} -N _{1DBU} , C _{CO₂} -N _{2DBU} , (d) O _{CO₂} -N _{1DBU} , O _{CO₂} -N _{2DBU} , (e) C _{CO₂} -O _{DMSO} , C _{CO₂} -S _{DMSO} (f) O _{CO₂} -O _{DMSO} , O _{CO₂} -S _{DMSO} in Eth+DBU+DMSO+CO ₂ system. N _{1DBU} , N _{2DBU} are sp ³ and sp ² hybridized nitrogen atoms of DBU, respectively. O _{DMSO} and S _{DMSO} are oxygen and sulfur atoms of DMSO, respectively.	100

Scheme 3.2	Pictorial representation of the constituent species orientation around CO ₂ for (a) Eth+DBU+CO ₂ and (b) Eth+DBU+DMSO+CO ₂ systems. Hydrogens attached to carbon are not shown for clarity. Here, bonds of Ch ⁺ , EG, and DBU molecules are depicted in ice blue, mauve, and cyan colors, respectively. Here, Ch ⁺ , EG, DBU and DMSO species within 4.4 Å and 4.8 Å of residue CO ₂ are shown in Eth+DBU+CO ₂ and Eth+DBU+DMSO+CO ₂ systems, respectively. Nearest Cl ⁻ from residue CO ₂ are shown in the scheme. The color coding of the atoms is the same as represented in Scheme 3.1.	101
3.6	RDFs depicting correlation for (a) HO _{[Ch]⁺} -Cl ⁻ , (b) HO _{EG} -Cl ⁻ , (c) HO _{[Ch]⁺} -OH _{EG} , (d) N _{[Ch]⁺} -Cl ⁻ , (e) HO _{EG} -OH _{[Ch]⁺} , (f) N _{[Ch]⁺} -OH _{EG} , (g) HO _{EG} -N _{1DBU} , HO _{EG} -N _{2DBU} in Eth+DBU system, and (h) HO _{EG} -N _{1DBU} , HO _{EG} -N _{2DBU} , (i) HO _{[Ch]⁺} -O _{DMSO} , HO _{[Ch]⁺} -S _{DMSO} and (j) HO _{EG} -O _{DMSO} , HO _{EG} -S _{DMSO} atomic pairs in Eth+DBU+DMSO system.	102
3.7	CV in Ar and CO ₂ saturated electrolytes in each of the solvent systems (a) Ethaline (b) Eth:DBU (9:1) (c) Eth:DBU (9:1)-DMSO and (d) Eth:DMSO:DBU (4:4:2).	104
3.8	(a) CVs of the CO ₂ saturated DESs based solvents, (b) Comparison graph of current density at -2V vs Ag QRE and conductivity. EIS comparison curves at (c) OCP, and at (d) -1.5 V vs Ag QRE, (d) differential capacitance vs potential curves of the DES based solvents.	105
3.9	Normalized differential capacitance curves of the solvent systems studied in the chapter.	103
3.10	(a-c) faradaic efficiencies of CO ₂ reduction products in each solvent system. (d) Repetitive cycles of CO ₂ capture (30 min.) and electrochemical CO ₂ conversion (2 hr) in Eth:DBU(9:1)-DMSO at room temperature and 50°C. (e) CO ₂ reduction products cumulative production rate for each of the solvents at different potentials.	105
3.11	(a) Comparison of CO ₂ capture capacity of Ethaline and 1M ChCl:DMSO, (b) Product profile of the electrochemical reduction of CO ₂ and (c) Repetitive cycles of CO ₂ capture (30 min.) and electrochemical CO ₂ conversion (2 hr) in 1M ChCl:DMSO.	106
3.12	(a) CO ₂ capture capacity (b) electrochemical CO ₂ reduction efficiency of pure Eth and systems with deliberate water addition in Eth	112
3.13	¹ H NMR of fresh and spent (a) Eth, (b)Eth:DBU (9:1) and (c) Eth:DBU (9:1)-DMSO.	113
3.14	SEM images Cu foil (a) electropolished (b) dipped in DES overnight and (c) Cu foil post electrolysis. (d) corresponding XRD patterns.	114

3.15	(a) Capture to conversion comparison, (b) Cdl of the DES based systems at OCP and negative polarization of -1.5V vs Ag QRE (c) schematic representation of the EDL structures in the three DES based systems and (d) Proposed electrochemical interfacial structure in Eth, Eth:DBU(9:1) and Eth:DBU(9:1)-DMSO solvents to understand the approach of captured CO ₂ molecule.	115
4.1	FTIR analysis of the DESs, vis., (a) ChCl:Bu, (b) ChCl:Cr, (c) ChCl:LV, and (d) ChCl:Ph along with its constituents to analyse the H-bonding interaction.	129
4.2	¹ H NMR analysis of the DESs, vis., (a) ChCl:Bu, (b) ChCl:Cr, (c) ChCl:LV, and (d) ChCl:Ph along with its constituents to analyse the H-bonding interaction.	131
4.3	(a) The CO ₂ absorption capacity of the DESs measured gravimetrically and (b) Free volume% of the as prepared DES and its comparison to their CO ₂ capture capacity	132
4.4	In-situ IR graphs to understand the CO ₂ capture state and interactions in DES (a) ChClBu, (b) ChClCr, (c) ChClLV and (d) ChClPh.	133
4.5	CV curves of Ar (dot-dashed lines) and CO ₂ saturated DESs (solid lines): (a) ChCl:Bu, (b) ChCl:Cr, (c) ChCl:LV, and (d) ChCl:Ph.	134
4.6	(a) CV and (b) EIS curves at OCP measured in CO ₂ -saturated DES. Comparison of (c) current density at -2V vs Ag QRE vs conductivity of DES. (d) Change in charge transfer resistance with respect to the potential.	135
4.7	FE for CO (solid columns) and H ₂ (lined columns) and CO yield rate (on right Y-axis) at varying applied potentials for each of the DESs; (a) ChCl:Bu, (b) ChCl:Cr, (c) ChCl:LV, and (d) ChCl:Ph.	136
4.8	Rate of CO ₂ capture and subsequent conversion for three repetitive consecutive cycles in (a) ChCl:Bu (b) ChCl:Cr (c) ChCl:LV and (d) ChCl:Ph.	137
4.9	Chronoamperometry of CO ₂ loaded ChCl:Ph solvent for 5 hrs. at -1.8 V vs Ag QRE.	138
4.10	Chronoamperometry at -1.8V vs Ag QRE of Ar saturated solvent as control experiments to understand the source of carbon and to detect any solvent degradation. (Inset shows GC-TCD and FID for the gas analysis and NMR-pre and post electrolysis of the solvents to detect any solvent degradation) (a) ChCl:Bu, (b) ChCl:Cr (c) ChCl:LV and (d) ChCl:Ph.	136
4.11	¹ H NMR of fresh and spent catholyte after 2 hrs. of CO ₂ electrolysis at -2 V to check for formation of any liquid products and the stability of	137

	electrolyte. Inset shows pictures of vials with fresh and spent electrolyte to depict any colour changes post-electrolysis.	
4.12	(a) A relationship between CO ₂ capture capacity and its conversion efficiencies, (b) C _d vs E curves in the faradaic region, (c) current response plots to find out the diffusion coefficient of CO ₂ , and the corresponding (d) Cottrell diffusion current density vs $t^{-1/2}$ (s ^{-1/2}) curves for CO ₂ electroreduction for different DES systems.	138
5.1	(a) XRD diffractograms and (b) Raman spectra of Cu electrodeposits	155
5.2	SEM images of the Cu electrodeposits obtained with different Cu-salt anions: (a) CC, (b) CS, (c) CA, and (d) CN.	156
5.3	The fitted Cu 2p XPS spectra of (a) CA (b) CC (c) CN and (d) CS.	157
5.4	The fitted O1s XPS spectra of (a) CA (b) CC (c) CN and (d) CS.	159
5.5	TGA curves of the Cu electrodeposits.	160
5.6	(a) LSV and (b) EIS at -0.83 V of CC in Ar and CO ₂ purged solutions. (c) LSVs and (d) EIS at OCP of each Cu catalyst in CO ₂ saturated solution for comparison. (R _s - solution resistance, R _{ct} - charge transfer resistance, C - constant phase element)	161
5.7	(a) EIS at OCP of CA, CC, CN, CS in 0.1 M HClO ₄ to find C _{dl} of each of the catalysts and (b) CV curves of the catalysts normalised by ECSA.	162
5.8	(a) ECR product profile and (b) selectivity towards Carbon-products on Cu-electrodeposits at -0.83 V. ECR product profile at varying potentials for (c) CC and (d) CS.	164
5.9	CA curves of (a) CC and (c) CS. XRD patterns of (b) CC and (d) CS electrodeposits on CFP before and after stability run. (*on XRD peaks corresponding to CFP).	165
5.10	Cu 2p and O 1s XPS spectrum of CC electrocatalyst before electrolysis ((a)and (c)) and after electrolysis for 7 hrs ((b) and (d))	166
5.11	SEM images of pre- and post-electrolysis samples of (a) CC and (b) CS.	167
5.12	A schematic representation of the probable mechanistic pathway on the cubic Cu (100) surfaces formed on the CC electrocatalyst.	168
5.13	(a) SEM images of the pre- and post-electrolysis electrocatalyst CC in Ethaline (b) Chronoamperometry of upto 3000s on CC in Ethaline	171
6.1	HQSC NMR of the lignin used in the work.	184

6.2	(a) CV curves of Sn electrode in Ar and CO ₂ saturated electrolyte (inset: change in peak current densities with respect to scan rate) (b) Faradaic efficiency and yield rate of formic acid at various potentials	186
6.3	(a) CV curves in 1M KOH with and without lignin (inset: change in peak current densities with respect to scan rate) (b) product profile of lignin depolymerisation products.	187
6.4	Electrochemical performance of the 2-electrode system: Ni-KOH-LOR_Sn-KHCO ₃ -ECR (a) LSV curves for the electrolyser set-up with varying oxidation and reduction processes as shown, (b) faradaic efficiency and yield of formic acid at the various cell potentials and (c) Yield % of lignin depolymerised monomers at given cell potentials.	188
6.5	(a) CV curves in Ar and CO ₂ saturated Ethaline (inset – peak current vs scan rate graph) (b) Faradaic efficiency and yield rate of formic acid form captured CO ₂ in Ethaline.	189
6.6	(a) CV and (b) chronoamperometry at 0.5V vs Ag QRE of lignin depolymerisation in KOH-DES mixtures.	190
6.7	Electrochemical performance of the 2-electrode system: Ni-KOH-LOR_Sn-Eth-ECR (a) LSV curves for the electrolyser set-up with varying oxidation and reduction processes as shown, (b) faradaic efficiency and yield of formic acid at the various cell potentials and (c) Yield % of lignin depolymerised monomers at given cell potentials.	191
6.8	(a) LSV curves for the electrolyser set-up with varying oxidation and reduction processes as shown in the DES-DES cell set-up. (b) Faradaic efficiency and yield of formic acid at the various cell potentials and (c) Yield % of lignin depolymerised monomers at given cell potentials in the Ni20KOHeth-Lig_Sn-Eth-CO ₂	192
6.9	Electrochemical performance of electrolyser system (a) Linear sweep voltammetry of the coupled lignin depolymerization and electrochemical CO ₂ reduction in DES-DES and DES-aq system (b) Electrochemical CO ₂ reduction product profile in the Ni-20KOHeth-LOR_Sn-Eth-ECR (c) Electrochemical lignin oxidative depolymerisation (LOR) reaction in the Ni-20KOHeth-LOR_Sn-Eth-ECR.	193
6.10	SEM images of Ni foam (a) pre-electrolysis, (b) post electrolysis in KOH and (c) post electrolysis in Ethaline. Inset of the SEM shows the zoomed image of the corresponding electrodes.	194

6.11	SEM images of Sn foil (a) pre-electrolysis, (b) post electrolysis in KHCO_3 and (c) post electrolysis in Ethaline. Inset of the SEM shows the zoomed image of the corresponding electrodes.	195
7.1	A key schematic representation of the key future perspectives as proposed in the thesis	210
A1.1	^1H NMR of the (a) ethylene glycol, (b) choline chloride, and (c) DBU.	211
A1.2	Relative amount of alkyl carbonates in Eth:DBU based solvent systems calculated with respect to phenol as internal standard	212
A1.3	(a) Calibration of Ag wire against a decamethyl ferrocene/decamethyl ferrocenium ($\text{dmFc}/\text{dmFc}^+$) redox couple	213
A1.4	(a) CV with potential calibrated against ($\text{dmFc}/\text{dmFc}^+$) redox couple (b) iR corrected CV curves of the DES systems.	213
A1.5	Current density vs time data during chronoamperometry experiments in each of the solvent system at different potentials.	214
A1.6	(a) GC-FID signal for the blank experiment (CO_2 reduction where anolyte and catholyte is ethaline) (b) GC-FID signal for electrolysis in CO_2 captured solvent.	214
A2.1	(a) FTIR curves before (dotted lines) and after CO_2 capture (solid lines) and (b) NMR of DES before (lighter shade) and after CO_2 capture (darker shade).	215
A2.2	EIS spectra at -1.4V, -1.6V and -1.8V vs Ag QRE in (a) ChCl:Bu, (b) ChCl:Cr, (c) ChCl:LV and (d) ChCl:Ph	216
A2.3	(a) Overlay of CV curves of ferrocenium couple in each of the DES solvents. (b) Overlay of CV of ferrocenium couple in Acetonitrile referenced with Ag wire and Ag/AgCl/ Cl^- .	217
A3.1	EDX analysis of the Cu-electrodeposits.	219
A3.2	Left panel) XPS survey scan for the Cu catalyst along with (right panel) the enlarged view of the curve from 555 to 590 eV showing the Cu $\text{L}_{3\text{M}_{4,5}\text{M}_{4,5}}$ Auger peak at ca. 571 eV.	220
A3.3	(a)FTIR and (b-c) C1s – XPS of CC and CS catalysts	221
A4.1	CV with increasing scan rates to characterize the redox peaks in (a) Sn foil in KHCO_3 , (b) Ni in KOH and (c) Sn foil in Ethaline.	222
A4.2	(a) CV curves of Ni foam electrode in 20KOHeth electrolyte, with and without lignin (b) Yield % of the lignin monomers with various potentials	223
A4.3	Control experiments - (a) comparison of lignin depolymerisation in KOH at room temperature, 50°C and of lignin functional unprotected by propionaldehyde, (b) comparison of lignin depolymerisation in Ethaline at room temperature and at 50°C , (c) comparison of electrochemical CO_2	224

	reduction in KHCO_3 at room temperature and at 50°C and (d) comparison of electrochemical CO_2 reduction in Ethaline at room temperature and at 50°C .	
A4.4	Chronoamperometry curves of (a) Ni-KOH-LOR_Sn-KHCO3-ECR system (b) Ni-KOH-LOR_Sn-Eth-ECR and (c) Ni-20KOHeth-LOR_Sn-Eth-ECR	225

LIST OF TABLES

Table No.	Table caption	Page No.
1.1	CO ₂ reduction reactions for various products and their corresponding thermodynamic energies and potentials.	8
2.1	The composition of various DES systems used in the thesis.	42
2.2	Products obtained by the electrochemical cleavage of kraft lignin at a foam stack electrode after 2 hr of electrolysis, <i>via</i> GC-MS	76
3.1	EIS fitting parameters and C _{dl} values of the EIS curves of Figure 3.9 (c and d)	106
3.2	Water content at various steps of the electrolysis experiment	111
3.3	Summary of the representative reports on electrochemical CO ₂ reduction to compare the yield rate of the work.	117
3.4	Summary of the representative reports on CO ₂ capture solvents used as electrolytes electrochemical CO ₂ reduction reaction.	119
4.1	Physico-chemical properties of the DESs analyzed in the present study.	128
4.2	Potential of E ⁰ and E _z in each of the DES vs NHE and Ag QRE.	143
4.3	The value of Cottrell slope and diffusion coefficient of CO ₂ calculated by the Cottrel and Wilke-Change equation	146
5.1	A summary of important physico-chemical properties, viz. morphology, dominant crystallographic phases from XRD, metal oxide content from XPS, along with roughness factor and FE for multi-carbon products from electrochemical measurements.	155
5.2	Summary of the representative reports on ECR on Cu nanocubes and oxide derived Cu electrocatalyst.	169
6.1	Concentration of surface adsorbed species (oxide states) calculated from the Brown-Anson equation.	197
6.2	Summary of the representative reports on electrochemical lignin oxidative depolymerisation.	198
7.1	The following table provides a centralised summary of the relevant key figures of merit for integrated CO ₂ capture and conversion technology.	207
A2.1	Electrochemical circuit fit parameters of EIS at OCP.	215
A3.1	Metal content of the electrodeposits estimated via ICP-MS measurements and Cu 2p XPS peak positions and its Cu ²⁺ /Cu ⁺ -Cu ⁰ ratios, O 1s XPS peak position and its relative % of lattice O (Cu-O) in different samples.	218

LIST OF ABBREVIATIONS

Abbreviation	Full Form
AFM	Atomic Force Microscopy
CCS	CO ₂ Capture and Storage
CCU	CO ₂ Capture and Utilisation
CFP	Carbon Fibre Paper
CPE	Constant Phase Element
CV	Cyclic Voltammetry
DAC	Direct Air Capture
DBU	1,8-Diazabicyclo[5.4.0]undec-7-ene
DD	Double Distilled
DEA	Diethanolamine
DGA	Diglycol-amine
DES	Deep Eutectic Solvents
ECR	Electrochemical CO ₂ Reduction
ECW	Electro-chemical Window
EDL	Electrochemical Double Layer
EIS	Electrochemical Impedance Spectroscopy
eRCC	Electrochemical Reactive CO ₂ Capture
FTIR	Fourier Transform Infra-red Spectroscopy
GC	Gas Chromatogram
HBA	Hydrogen Bond Acceptor
HBD	Hydrogen Bond Donor
HER	Hydrogen Evolution Reaction
IL	Ionic Liquid

KF Titration	Karl Fischer Titration
LSV	Linear Sweep Voltammetry
MEA	Monoethanolamine
MEA	Membrane electrode assembly
MDEA	N-Methyldiethanolamine
MOF	Metal Organic Framework
NMR	Nuclear Magnetic Resonance
OCP	Open Circuit Potential
OER	Oxygen Evolution Reaction
PEM	Proton Exchange Membrane
PZC	Potential of Zero Charge
QRE	Quasi Reference Electrode
RCC	Reactive CO ₂ Capture
RDS	Rate Determining Step
STM	Scanning Tunneling Microscopy
SEM	Scanning Electron Microscopy
TEM	Transmission Electron Microscopy
XRD	X-Ray Diffractogram